Filtering Antenna-to-Antenna Reflections in Antenna Extrapolation Measurements[1]

Robert D. Horansky, Mohit S. Mujumdar, Dylan F. Williams, Kate A. Remley, Joshua A. Gordon, David R. Novotny, Michael H. Francis
Communications Technology Laboratory
NIST
Boulder, CO USA
horansky@nist.gov

***Abstract*—To provide modulated-signal traceability into the free-field, we are extending the three-antenna, extrapolation method used for on-axis antenna gain, from using only scalar data, to using the full magnitude and phase information between the antennas. We have examined several aspects of the extrapolation fitting, such as averaging of the data and the stability of fitting methods. Here, we will present our simulation result showing that, in our antenna range, filtering of reflections between antennas is an unnecessary step in the extrapolation method.**

I. Introduction

Within the communications field, there is a large breadth of wireless devices that require characterization and testing. These tests may be for metrics such as antenna pattern, as well as full signal path metrics such as receiver sensitivity. With the shrinking size of mobile devices, as well as the use of multiple antennas, many wireless devices are foregoing test ports for separately characterizing the antennas, receivers and transmitters. The use of a test cable may change the behavior of a device antenna negating the meaningfulness of conducted-device testing. As such, the use of over-the-air (OTA) testing has become ubiquitous for mobile wireless devices with many of the relevant metrics requiring a communication link with the device under test.

Since OTA tests dominate the measurements of wireless devices, and given the variety of techniques to conduct these measurements, there is a paramount need for a meaningful way to compare measurements between setups. Many metrics, such as receiver sensitivity, require demodulation of a communication signal. Thus, both the phase and magnitude of a reference field are necessary. At NIST, we have developed a connectorized, wide-band, precision, modulated-signal source [1]. The waveforms generated by the source and the related uncertainties are traceable to primary standards. Accurately characterizing the magnitude and phase of the on-axis gain of the antennas is the next step to creating known modulated signals in a free-field environment, and motivates the present work.

The traceability path for a conducted signal at millimeter-wave frequencies is described in Ref. [1]. The traceability is provided using a calibrated sampling oscilloscope as the receiver to both verify the modulated signal and predistort it to correct for hardware errors. The sampling oscilloscope is traceable to primary standards where all uncertainties and any correlations between the uncertainties are tracked in every step of the measurement process through an in-house software suite called the NIST Microwave Uncertainty Framework [2].

To extend this traceability from the connectorized source into free-space, as shown in Fig. 1, we need to include in the traceability chain the scattering matrix of a radiating antenna, and the correlated uncertainties required for modulated-signal traceability. We have started doing this with on-axis measurements, with a planned extension to off-axis patterns. We will discuss the correlated uncertainties elsewhere.

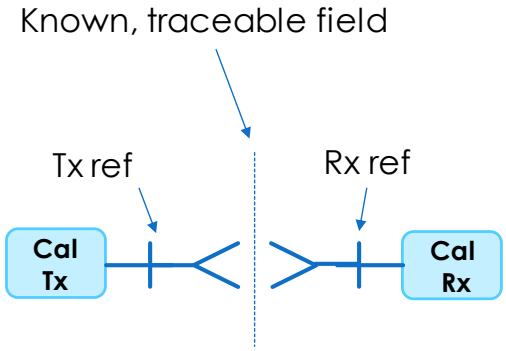

Figure 1: The goal of the work presented here is to provide a precision, free-field modulated signal source, traceable to primary standards. This will be accomplished by using a calibrated transmitter, shown on the left, and the known antenna scattering parameters, to provide the traceable signal shown at the dotted line located anywhere between the two antennas. We can verify this field with a calibrated receiver such as an equivalent-time sampling oscilloscope shown on the right. In both cases, we require fully calibrated antennas to transform the connectorized reference planes "Tx ref" and "Rx ref" to the free-field between the antennas.

Currently, on-axis, far-field gain of an antenna is provided by using a three-antenna extrapolation measurement. This is achieved by measuring the pair gain of at least three permutations of the antenna pairs. We can then extract the individual gain of each antenna without having to rely on a known reference antenna [3].

Since it is difficult to measure pair gain in the far field, either due to space limitations or low signal levels, the pair gain is currently fit as a function of antenna distance in the near-to-mid-field regime at NIST. This has traditionally been done at NIST using scalar measurements of the transmission coefficients between the two antennas as a function of their separation distance. *However, for a free-field modulated signal source, we need the full complex scattering-parameter matrix of the antenna*. Thus, in this work, we are extending the extrapolation method to use the full complex transmission coefficient S_{21} obtained from the pair measurement, as also proposed in Refs. [4,5].

In the process of fitting the complex transmission coefficients, we have examined some of the algorithm choices that have traditionally been used in the extrapolation method. To aid us in our analysis, we created a simulated data set to compare algorithm steps. Here we present an example of one such study looking at the use of filtering to remove the presence of multiple reflections between antenna pairs.

In this paper, we will first discuss how extrapolation measurements are currently done and the algorithm for fitting the data. Then we will show the simulations that we performed to analyze the effect of filtering on the extrapolation fits. Finally, we show results that suggest filtering at reflection magnitudes relevant to experimental values is not required in our range at the distances we use to perform the extrapolations, and may cause degradation in the accuracy of some measurements.

II. NIST Extrapolation Measurements

A. Pair Gain Using Power Fits

When NIST provides antenna gain to a customer, the result comes from the three-antenna, extrapolation measurement, which provides the on-axis antenna gain. The antenna gain can then be used to normalize pattern measurements.

The extrapolation measurement is performed with a vector network analyzer (VNA), which measures the scattering parameters of each pair of antennas, and is carried out as a function of distance between them. When the extrapolation method was first developed, phase measurements were either not possible, or the uncertainty was much higher than for measuring power. Therefore, the algorithms developed for fitting an expansion to the extrapolation measurements were based on total power transmitted between the two antennas (*i.e.* the square of the magnitude of the transmission coefficient $|S_{21}|^2$), as a function of distance between the antennas. At the time, this allowed lower uncertainties, but ignored phase information.

The distance in the extrapolation measurement is now provided by the NIST CROMMA system, which is an articulated robotic arm that provides very accurate position measurements, which is especially beneficial at millimeter-wave frequencies. Furthermore, with modern instrumentation, we can perform very precise measurements of the relative phase between the two antennas [6]. We bring those two together here to measure both the magnitude and phase of pair gain.

In the absence of reflections between the antennas, the dependence of the transmission coefficient S_{21} with distance $\bar{r} = r - r_0$ is given by,

$$S_{21} = \frac{e^{ik\bar{r}}}{\bar{r}}\left(A_{00} + \frac{A_{01}}{\bar{r}} + \frac{A_{02}}{\bar{r}^2} + \frac{A_{03}}{\bar{r}^3} + \cdots\right), \tag{1}$$

where r is the distance between the antennas and r_0 sets the origin of the expansion used in (1). This is typically determined geometrically and set to 0. The A_{0n} terms are the coefficients of the expansion and $k = \frac{2\pi}{\lambda}$, with λ being the wavelength of the measurement. The first-order series in (1), multiplied by $\frac{e^{ikr}}{\bar{r}}$, represents the unreflected transmission coefficient between the antennas being measured. The leading term A_{00} is the dominant term in the far-field, and the other A terms in the first-order series correct for the near- to mid-field behavior [7]. The magnitudes of a typical NIST extrapolation data set are shown in blue in Fig. 2. We are using a measurement done at 118.75 GHz between a $\mu = \pm 1$ probe antenna with a nominal gain of 8 dB, and a standard gain horn with nominal gain of 15 dB. The dominant antenna aperture, D, is from the horn antenna and is 0.0248 m. In eq. (1), the A terms are complex providing two fit parameters each in the fitting procedure. The goal in the extrapolation measurement is to extract only the first order series to determine the A_{00} term, which will then provide far-field behavior [3].

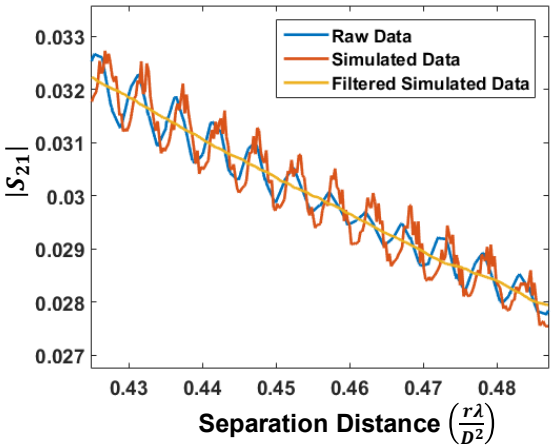

Figure 2: Example of an extrapolation measurement between a $\mu = \pm 1$ probe antenna and a standard gain horn at 118 GHz. The raw data are shown in blue versus the distance normalized by D^2/λ. The simulated data with the magnitude of ripples chosen to match the raw data and noise are shown in red. The sinc filtered model data are shown in yellow.

Reflections between the antennas introduce higher-order terms in the series. While the reflections are complicated, and may originate at several different distances, to first order, they can be represented with additional terms of the form $\frac{e^{3ikr}}{\bar{r}^3}$ and $\frac{e^{5ikr}}{\bar{r}^5}$, representing reflections that traverse three times and five times the distance of the first order series. The resulting expression is

$$S_{21} = \frac{e^{ikr}}{\bar{r}}\left(A_{00} + \frac{A_{01}}{\bar{r}} + \frac{A_{02}}{\bar{r}^2} + \frac{A_{03}}{\bar{r}^3} + \cdots\right)$$
$$\frac{e^{3ikr}}{\bar{r}^3}\left(A_{10} + \frac{A_{11}}{\bar{r}} + \frac{A_{12}}{\bar{r}^2} + \cdots\right) + \frac{e^{5ikr}}{\bar{r}^5}\left(A_{20} + \frac{A_{21}}{\bar{r}} + \cdots\right) + \cdots, \quad (2)$$

We use the higher-order terms A_{10} and A_{20}in (2) to simulate multiple reflections in our range. The first order series in (2) is a function whose magnitude is monotonically decreasing, while the higher order series impart a ripple on top of this decreasing behavior, as can be seen in Fig. 2. A simulation using eq. (2) is shown in red in Fig. 2.

When power is used for the extrapolation measurement, we must then use the squared magnitude of eq. (1). There will be complex ripple terms from the higher order series, but the first order series will yield,

$$|S_{21}|^2 \approx \frac{1}{\bar{r}^2}\left(A'_{00} + \frac{A'_{01}}{\bar{r}} + \frac{A'_{02}}{\bar{r}^2} + \frac{A'_{03}}{\bar{r}^3} + \cdots\right), \quad (3)$$

where the A' terms now represent scalar quantities. The far field term has a simple relation back to the vector quantity given by,

$$A'_{00} = |A_{00}|^2, \quad (4)$$

and is proportional to the far-field pair gain.

The previous NIST algorithm for fitting the extrapolation data and extracting the pair gain uses the work flow shown in Fig. 3. The raw S_{21} data are converted to transmitted power-like quantity, which destroys the phase information. Next, a distance gate is applied to the power-like data to remove effects from near-field behavior, typically around $2D^2/\lambda$. This also removes data from too large a distance where external reflections and poor signal-to-noise are problematic. Then, a boxcar filter the width of the excitation wavelength is applied to the raw data to remove the multiple reflections. The fourth step is an averaging of the smoothed data to improve processing time. Next, the data are normalized by $\lambda r/D^2$, where λ is the wavelength being measured, r is the distance between the antennas, and D is the larger antenna aperture. The square of the normalization factor

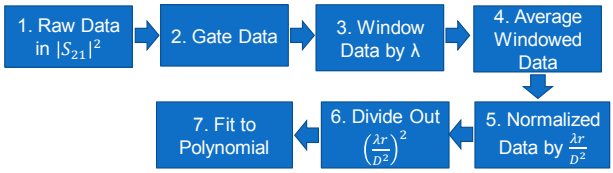

Figure 3. Algorithm used to extract far-field pair gain from an extrapolation measurement that fits the measured power transmitted between the antennas.

is divided out of eq. (3). This removal of the normalization has the effect of giving greater weight in a least-squares fit to data at longer distances by a factor of r^2. Also, the normalization step allows the extrapolation to be fit by a polynomial, which is computationally faster.

B. Pair Scattering Using Magnitude and Phase

Since the primary goal of this work is to extend traceability from a conducted precision communication signal to a free-space signal, both magnitude and phase information are necessary to allow demodulation. In the process of adapting the work flow of Fig. 3, we studied the necessity of several of the steps. In fitting the complex data, we use the raw scattering-parameter measurements in step 1. The gating in step 2 is accomplished by using data where the relative phase between the antennas is linear. The windowing of step 3 will be shown in the next section in Fourier space. Step 4 reduces the amount of data with averaging, but is no longer necessary since modern computing power can easily handle the amount of extrapolation data that is taken. The normalization in step 5 is accomplished by weighting the least squares fit by r for complex data, or if power-like data are used, r^2. Finally, we found that fitting to a polynomial was only marginally faster than fitting the series in eq. (1) explicitly. Also, when fitting the series explicitly, we can adjust the origin r_0 of the expansion if desired. This allows exploration of the effect of changing the origin of the expansion on the resultant pair gain or scattering matrix.

III. Simulated Data

We are interested in exploring the necessity of the windowing step in the extrapolation method. Since we are using the full complex data, the windowing in r-space is equivalent to applying a sinc filter in k-space (inverse r-space). We decided to explore the usefulness of the filtering step by creating data with (2) where we know the A_{00} term and could compare the fitted results to that value.

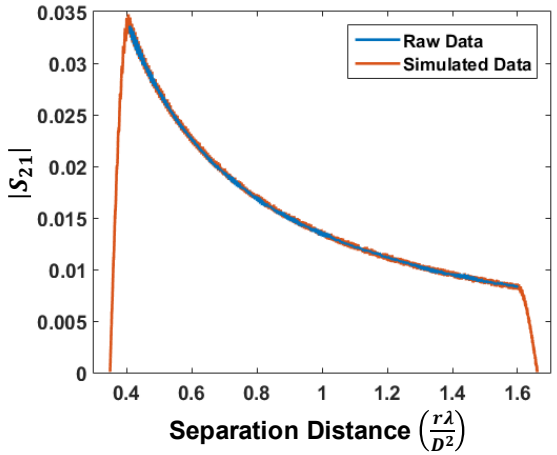

Figure 4. The raw extrapolation data (blue) used for creating the model data. The simulated data used for the filtering experiment are shown in red. The simulated data extends further in distance due to the buffers used at the end of the data to smooth the Fourier transform and reduce side lobes.

By starting with the values for the A terms extracted from a least-squares fit of eq. (2) to the raw data shown in Fig. 2, we created simulated data that included higher-order terms that approximated the ripples we observed in our measurements. The simulated data contain four terms in the first-order series, one term for the third order-series, A_{10}, and one term for the fifth-order, A_{20}.

The raw data shown in Fig. 2 came from six measurements moving the antennas apart then together, three times each. We used the minimum and maximum distances and evenly spaced the model data using the same number of points as the 6 raw data runs combined, then added additional buffer points on both sides of the data. The buffers were then smoothly decreased to zero with a sinusoidal multiplier to allow a smooth Fourier transform of the data and reduce side lobes. The simulated data used is shown in Fig. 4, and compared to the raw data that were used as the starting point. A magnified version of the data is shown in Fig. 2.

The windowing that was done for the power data is accomplished for the complex data by filtering the Fourier transform of the simulated data. Figure 5 shows the Fourier transform of 100 copies of the simulated data, each with a different normally distributed random noise added to the data. The Fourier transform yields k as the x-axis, but this is converted to a frequency, f, by multiplying by the speed of light. Overlaid on the model data is the sinc filter, which is the Fourier transform of the boxcar window. Fig. 6 shows model data with the higher order reflections amplified to appear on a linear scale. The Butterworth filter, which we also simulated, is shown as well.

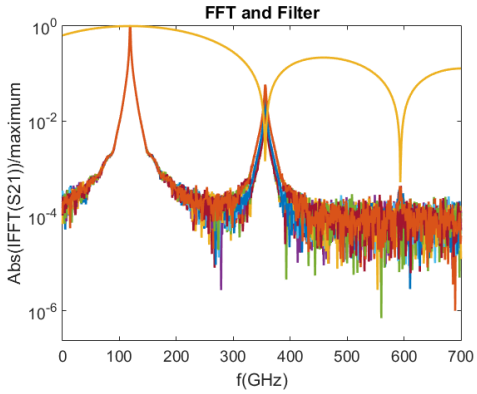

Figure 5: Plot of the simulated extrapolation data, with several levels of noise in Fourier space versus frequency, converted from inverse distance. Also shown, in yellow, is the sinc filter used to remove the higher-order reflections.

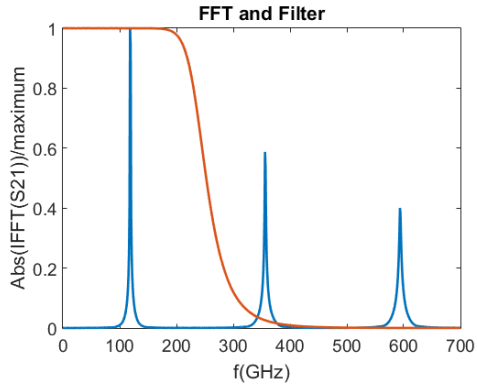

Figure 6: The model data Fourier transformed to k-space with the higher-order reflections made very large. In red is shown the Butterworth filter at a given cutoff.

IV. Results

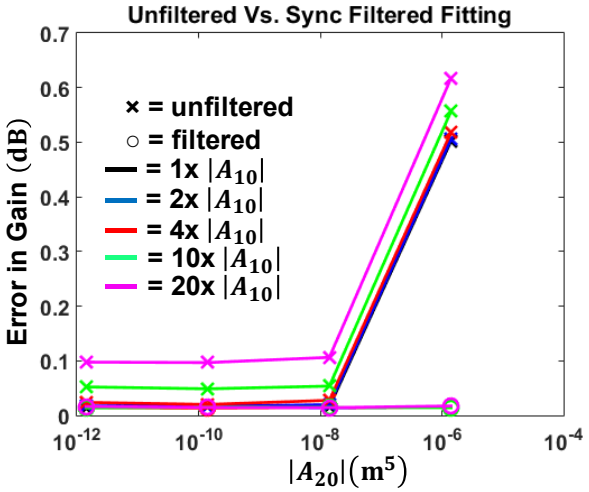

Figure 7: Plot of the relative error in the pair gain taken from the magnitude of the pair scattering compared to the value defined in model data. The error is plotted versus the magnitude of the fifth-order series term in the extrapolation expansion. The data represented with x's are the values taken from fits to unfiltered data. The open circles are filtered by a sinc function. The legend shows the multiplier of the third order term, where multiplying by one yields an oscillation magnitude equivalent to the measured data.

We compared the results of filtering the simulated data first against performing the least-squares fit without filtering. The magnitude of the third-order term, A_{10}, was increased from 0.5e-6 m^3, which yielded ripples of similar magnitude to experimental data, up to 1e-5 m^3. For each value of A_{10}, the magnitude of the fifth-order terms, A_{20}, was varied from 1e-12 m^5 to 1e-6 m^5. Finally, for each value of the third- and fifth-order magnitudes, 100 iterations of normally distributed noise were added to each point. The average of the resultant fits to the first-order series are shown as the data points in Figs. 7 and 8. Fig.7 shows the comparison between filtering with a sinc filter as shown in Fig. 5, while Fig. 8 shows the Butterworth filter comparison. The y-axis of the plot shows the relative error in the pair gain found from fitting the data over the 100 noise iterations, compared to the actual value defined in the model data. The x-axis shows the increasing magnitude of A_{20}. The plots with x's are the model data fitted with no filtering. The lines with circles show the relative error in the magnitude of the A_{00} term when filtered data is fitted. The increase magnitude of A_{10} is shown by the varying colors of the lines.

If we look at a single-color pair, we can see the effect of the fifth-order term. Only at very high values, over 10,000 times larger than what is observed in experimental data, filtering helps to reduce the error in the far-field, pair scattering parameter. Next, one can look at the progression of the different color lines. This is an increase in the third-order term, where the black plots are those for oscillations seen in the raw data in Fig. 2. At lower values of the third-order term, the filtering does not help lower the relative error in $|A_{00}|$. However, if a situation arises where the magnitude of the third-order term is 10x larger than seen in these raw data, then filtering could play a helping role in the analysis.

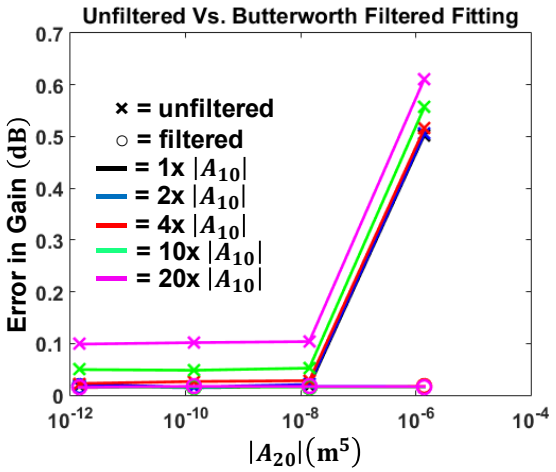

Figure 8: Plot of the relative error in the pair gain compared to the value defined in model data. The data was filtered using the Butterworth filter shown in Fig. 6.

V. Conclusion

We are extending NIST's traditional on-axis gain measurements to use the full complex scattering parameters we measure to determine complex pair-gain. This is a necessary step needed to extend a traceable modulated signal to free-space locations and be able to establish a traceable communication link to wireless devices. A traceable, free-space, modulated signal would allow calibration and comparison of OTA test methods across a broad range of frequencies and bandwidths.

In performing the extrapolation data fits, to find the far-field pair scattering parameter, we determined that filtering the reflections between the antenna pairs was unnecessary with the antennas we used in our range and at the distances we used in the fits. There may be cases where it becomes useful, perhaps at closer distances where the reflections are orders of magnitude higher that seen in this experimental, 118 GHz data. However, in the range of useful fitting, the ripples are filtered adequately in our data by the least-squares fit itself, and usually with less error than when filtering is used.

Our next step in the traceability process will be to incorporate this complex fitting into our uncertainty analysis software suite. We have already accounted for fitting and pointing errors and are currently incorporating calibration uncertainties for the VNA measurements. The next step will be to present the results of the full uncertainty analysis accounting for correlations for the far field scattering matrix of our radiating antenna.

References

[1] K. A. Remley, D. F. Williams, P. D. Hale, C.-M. Wang, J. Jargon, and Y. Park, "Millimeter-Wave Modulated-Signal and Error-Vector-Magnitude Measurement with Uncertainty," IEEE Trans. Microw. Theory and Tech., vol. 63, pp. 1710-1720, April 2015.

[2] D. F. Williams, "NIST Microwave Uncertainty Framework, Beta Version", NIST, Boulder, CO, USA, JJun. 2014 [Online]. Available: http://www.nist.gov/pml/electromagnetics/relate-software.cfm

[3] A. C. Newell, R. C. Baird, P. F. Wacker, IEEE Trans. Antenna Propagat., vol. 21, no. 4, July 1973.

[4] E. Van Lil, P. Govaerts, A. Van de Capelle, "Improved Extrapolation Methods for Antenna Gain Measurements," IEEE Microw Conf, 1990 20th Europe.

[5] P. F. Wacker, "Theory and numerical techniques for accurate extrapolation of near-zone antenna and scattering measurements", NBS Report 10 733, Apr. 1972.

[6] J. A. Gordon, D. R. Novotny, M. H. Francis, R. C . Wittmann, A.E. Curtin, M. L. Butler, and J. R. Guerrieri, "Millimeter-Wave Near-Field Measurements Using Coordinated Robotics," IEEE Trans. Antenna Propagat., vol. 63, pp. 5351-5362, October 2015.

[7] A. G. Repjar, A. C. Newell, and D. T. Tamura, "Extrapolation Range Measurements for Determining Antenna Gain and Poarization," NBS Tech Note 1311, August 1987.